



Determining Biophysical Parameters for Olive Trees Using CASI-Airborne and Quickbird-Satellite Imagery

J. A. Gómez,* P. J. Zarco-Tejada, J. García-Morillo, J. Gama, and M. A. Soriano

ABSTRACT

This study reports on the development of remote sensing methods for estimation of biophysical parameters in olive orchards. Field and airborne campaigns were conducted in 2003 and 2004 in two orchards located in southern Spain. Ground measurements of crown transmittance and leaf area index (LAI) of individual olive trees (*Olea europaea* L.) were done using the LAI-2000 Plant Canopy Analyzer. Hyperspectral images were acquired with a compact airborne spectrographic imager (CASI) at 1-m spatial and with QuickBird satellite sensor at 2.5-m spatial resolution. The panchromatic 0.6-m spatial resolution image was also acquired with QuickBird. These images enabled the application of automatic algorithms for olive crown identification and delineation, to determine tree crown size and LAI. These methods proved successful for determining projected olive crown area, obtaining determination coefficients (r^2) in the range of 0.82 to 0.65, and root mean square errors (RMSE) of 4.8 and 6.2 m² for CASI hyperspectral and QuickBird panchromatic images, respectively. The olive crown volume was estimated using image-estimated projected crown area values, yielding r^2 ranging between 0.87 and 0.70, with RMSE of 8.4 and 11.3 m³ for CASI hyperspectral and QuickBird panchromatic images, respectively. Olive crown transmittance and LAI of individual olive trees were evaluated using spectral vegetation indices (normalized difference vegetation index [NDVI], renormalized difference vegetation index [RDVI], simple ratio index [SR], modified simple ratio [MSR]) yielding better correlations with CASI images, r^2 in the range 0.71 to 0.75 ($P < 0.0001$) and 0.57 to 0.62 ($P < 0.0001$) for crown transmittance and LAI, respectively. These methods enable obtaining maps of biophysical parameters in olive trees at farm scale in an operational way demonstrating the validity of the methodology used.

OLIVE TREE IS the most widely cultivated tree crop in Mediterranean countries, where olive groves cover 8.6 million ha, ~93% of the world olive area (FAOSTAT, 2010). Among all the producing countries, Spain ranks first with 2.47 million ha of olive trees, of which 1.50 million ha are located in Andalusia; it's most Southern region (Consejería de Agricultura y Pesca, 2010).

Although their size varies slightly among varieties, olive trees grow in natural conditions 4 to 8 m height, forming a hemispheric tree crown. In olive plantations, tree crown size and shape, and leaf density and distribution are controlled by farmers through regular pruning (performed every 1–3 yr) to obtain a canopy structure best suited for optimum yield, prevention of pest and diseases, and to facilitate management of the plantation. To obtain the optimum crown size, farmers also take into account the tree density. Traditional rain-fed olive plantations have been cultivated with low plant densities (<100 tree ha⁻¹) to provide a large volume of soil, acting as a water reservoir, for each tree, and with one to four trunks per tree, subjected to frequent pruning to limit tree crown size. In recent decades, the expansion of irrigation has resulted in new

intensive plantations established with tree densities of 200 to 400 trees ha⁻¹, with only one trunk per tree; this has resulted in an increase of canopy cover but with tree crowns still spaced from each other. More recently, hedgerow plantations are being established, with smaller trees at very high densities up to levels approaching 2000 trees ha⁻¹, as a means of mechanization of harvesting operations (Pastor et al., 2007).

The tree crown size and the LAI, defined by Watson (1947) as the total one-sided area of leaf tissue per unit ground area (m² m⁻²), of olive canopies are key variables in hydrological and ecophysiological processes, controlling key environmental and agronomical issues. Olive biomass production and oil yield are closely related to the amount of photosynthetically active radiation (PAR) that is intercepted by leaves (Mariscal et al., 2000; Iniesta et al., 2009). Intercepted PAR is mainly determined by LAI (Monsi and Saeki, 1953); therefore, LAI is considered a critical input variable for simulation models of C and water fluxes in olive canopies. In the case of olive orchards, the intercepted PAR is regulated by the structure of the olive crown, and the density and orientation of the slopes where the orchard is grown (Mariscal et al., 2000). Hydrological processes are also regulated by the crown size and leaf area of olive trees. Interception of rainfall and funneling as stem flow by the olive canopy increases with increasing leaf area of trees (Gómez

J.A. Gómez, P.J. Zarco-Tejada, J. García-Morillo, and J. Gama, Instituto de Agricultura Sostenible (IAS), Consejo Superior de Investigaciones Científicas (CSIC). Apdo. 4084, 14080 Córdoba, Spain; M.A. Soriano, Departamento Agronomía, Universidad de Córdoba. Apdo. 3048, 14080 Córdoba, Spain. Received 5 Jan. 2011. *Corresponding author (joseagomez@ias.csic.es).

Published in *Agron. J.* 103:644–654 (2011)

Published online 28 Mar 2011

doi:10.2134/agronj2010.0449

Copyright © 2011 by the American Society of Agronomy, 5585 Guilford Road, Madison, WI 53711. All rights reserved. No part of this periodical may be reproduced or transmitted in any form or by any means, electronic or mechanical, including photocopying, recording, or any information storage and retrieval system, without permission in writing from the publisher.

Abbreviations: CASI, compact airborne spectrographic imager; cA, crown projection areas; cA', image-estimated crown projection areas; cV', image-estimated crown volumes; LAD, leaf area density; LAD_O, leaf area density of individual olive trees; LAI, leaf area index; LAI_O, leaf area index of individual olive trees; MSR, modified simple ratio; NDVI, normalized difference vegetation index; PAI, plant area index; PAI_O, plant area index of individual olive trees; PAR, photosynthetically active radiation; PCA, plant canopy analyzer; RDVI, renormalized difference vegetation index; SR, simple ratio index; SVI, spectral vegetation index; T_O, crown transmittance of individual olive trees.

et al., 2001). An increase of the ground cover by the olive crown results in a reduction of soil erosion risk (Gómez et al., 2003).

The ability to measure or estimate leaf area in olive orchards is critical to accurately model ecophysiological and hydrological processes, as well as orchard productivity. The major ground-based methodologies for estimating LAI use either direct measures through destructive sampling of the vegetation, or indirect methods involving optical instruments and models (Norman and Campbell, 1989; Bréda, 2003; Jonckheere et al., 2004; Weiss et al., 2004). Destructive sampling is time-consuming and expensive in tree crops, and sometimes not feasible (Villalobos et al., 1995). Alternative optical methods are based on the measurement of light transmission through canopies. These methods apply the Beer–Lambert law on the fact that the fraction of incoming radiation intercepted by a canopy depends on the canopy structure and optical properties (Monsi and Saeki, 1953). The LAI-2000 Plant Canopy Analyzer (Li-Cor, Lincoln, NE) is one of the most extensively used among the instruments for optical determination of LAI in broad-leaf and coniferous forests, for example, Gower and Norman, 1991; Stenberg et al., 1994; Cutini et al., 1998; Barr et al., 2004, and it has been calibrated and validated for use in olive trees by Villalobos et al. (1995). The primary disadvantage of these methods is that they yield information only for the immediate vicinity of the measurement points and considerable effort is required to obtain even the most local characterization of LAI.

Therefore, remote sensing makes progress on the development of methods to estimate canopy biophysical parameters, such as the canopy cover fraction and LAI, using sensors with different spatial and spectral characteristics. It is an area of active progress in the last decades aimed to provide extensive spatial information of the vegetation properties at different scales. Fassnacht et al. (1997) used the reflectance spectra of conifer, hardwood, and mixed conifer–hardwood forests derived from Landsat-5 Thematic Mapper (TM) to calculate vegetation indices that correlated r^2 from 0.60 to 0.75 with LAI measurements. Turner et al. (1999) evaluated the potential of three spectral vegetation indices (SVIs), NDVI, SR, and SAVI, using Landsat-5 TM, in areas with different vegetation (grass, shrubs, hardwood, and conifer forests), obtaining in general a high correlation between SVIs and LAI. The different types of vegetation showed differences on the predictive ability of the different SVIs, reflecting differences in the complexity of their structure and their spectral signature. Later, Haboudane et al. (2004) conducted an analysis based on both simulated and real hyperspectral data to compare performances of existing vegetation indices (NDVI, RDVI, MSR, SAVI, SARVI, MSAVI, TVI, and MCARI) and to design new ones (MTVII, MCARI1, MTVI2, and MCARI2) insensitive to chlorophyll content variations and linearly related to green LAI.

A new generation of hyperspectral satellite-based sensors, characterized by high spatial resolution (between 0.5 and 2.5 m) such as QuickBird (DigitalGlobe, Longmont, CO) or IKONOS (Space Imaging Corp., Thornton, CO) among others, provide an alternative to traditional imaging based on sensors of low spatial resolution and broad bandwidth. In particular, Laliberte et al. (2004) evaluated ground cover by shrubs and grass vegetation in New Mexico using aerial photography and QuickBird images with good results, and Johnson et al. (2003) used NDVI calculated from IKONOS images to determine LAI of vineyards in northern California obtaining a correlation of $r^2 = 0.72$.

Hyperspectral airborne sensors, such as airborne visible/infrared imaging spectrographer (AVIRIS; NASA Jet Propulsion Laboratory, California Institute of Technology, Pasadena, CA), compact airborne spectrographic imager (CASI; ITRES inc., Calgary, AB, Canada), airborne hyperspectral scanner (AHS; Daedalus Enterprise, WA), have also been used to evaluate biophysical properties of vegetation with high spatial resolution. In particular, work was conducted by Haboudane et al. (2004) using CASI airborne data for different crop types {soybean [*Glycine max* (L.) Merr.], corn [*Zea mays* L.], and wheat [*Triticum aestivum* L.]} at different growth stages and under various fertilization treatments. Prediction analysis of algorithms based on MCARI2 and MTVI2 resulted in agreements between modeled and ground measurement of nondestructive LAI, with coefficients of determination (r^2) being 0.98 for soybean, 0.89 for corn, and 0.74 for wheat, and corresponding RMSE values of 0.28, 0.46, and 0.85, respectively.

There is significantly less research on evaluation of biophysical properties of discontinuous vegetation canopies, such as in open-canopy tree crops, using remote sensing. The aggregation of pure crown, shadows, and soil background reflectance makes this situation more difficult to evaluate than in a homogeneous field crop providing full canopy ground cover. The use of hyperspectral sensors of high spatial resolution, airborne or satellite-based, provides the opportunity to evaluate the biophysical properties of individual trees and orchards, aiming at providing detailed maps at different scales of important environmental and agronomic traits, such as orchard productivity and soil erosion risk, and its temporal variation due to vegetation growth or phenological changes.

The objective of this study is to evaluate the potential of two high spatial resolution sensors, CASI and QuickBird, for determining and mapping the tree crown size, crown transmittance, and LAI of individual olive trees in commercial traditional and intensive olive plantations.

MATERIALS AND METHODS

Site Description

Ground and remote field measurements were made in two commercial olive orchards located in Andalusia, southern Spain, in summer 2003 and 2004. Both orchards differed in tree density, olive crown shape and size, and pruning, and were selected to obtain a broad range of planting conditions for validation purposes. The first orchard ('El Tobazo') is a traditional rain-fed olive orchard (cultivar Picual), ~100-yr old, planted at low tree density, 12 by 12 m tree spacing; since year 2000, some areas were interspersed with one-trunk irrigated olive trees, resulting in a 7 by 7 m tree spacing. The orchard is located in Alcaudete (Jaén province) over a mixed landscape of rolling hills and flat areas. The second orchard ('Alameda del Obispo') is an intensive irrigated olive orchard (cultivar Arbequina), 10-yr old at the time of the measurements, planted at high tree density, 3.5 by 7 m tree spacing, and is located in Córdoba on a flat landscape. The total number of olive trees measured was 86 in the orchard El Tobazo and 37 in the orchard Alameda del Obispo.

Furthermore, to explore the relationship between orthogonally projected crown area (cA) and crown volume (cV) in individual olive trees, six commercial olive orchards were selected from different geographical areas of Andalusia, to capture the variability of olive groves in the region. These olive orchards cover the main olive varieties (Picual, Hojiblanca, Manzanilla, and Arbequina)

Table 1. Location and characteristics of the commercial olive orchards where measurements were performed, all located in Andalusia region (Southern Spain).

Location (province) 'Olive orchard'	Orchard characteristics			Tree crown size		
	Tree density	Trunks per tree (number)	Olive variety	Olive trees measured (number)	Projected crown size (m ² ; range)	Crown volume (m ³ ; range)
Benacazón (Sevilla) 'Santa Marta'	6 × 8 m	1	Manzanilla	12	5.3–15.8	5.6–23.2
Almodóvar (Córdoba) 'La Conchuela'	6 × 7 m	1	Arbequina	12	6.2–15.9	7.9–21.8
Córdoba (Córdoba) 'La Granja'	6 × 6 m	1	Picual	12	12.0–26.4	15.7–46.2
Antequera (Málaga) 'El Huerto'	12 × 12 m	2–3	Hojiblanca	12	13.3–33.9	13.9–46.3
Bujalance (Córdoba) 'Parcelas 1–2'	12 × 10 m	2–3–4	Picual	12	18.2–32.8	28.0–46.8
Bujalance (Córdoba) 'Parcela 5'	10 × 10 m	1	Picual	6	19.5–24.6	17.3–26.7
<i>Experimental sites</i>						
Alcaudete (Jaén) 'El Tobazo'	12 × 12 m	2–3	Picual	71	10.1–39.6	14.6–80.5
	7 × 7 m	1	Picual	15	1.2–8.2	0.8–11.4
Córdoba (Córdoba) 'Alameda del Obispo'	3.5 × 7 m	1	Arbequina	37	3.1–9.3	3.6–28.7

characteristics of each area (or province), and planting systems (tree density and trunks per tree) and management (pruning, irrigation/rain-fed) generally used (Table 1). These differences in tree density, number of trunks per tree, pruning, and olive variety, provided a wide range in the crown size. The number of olive trees measured in each olive orchard, including the two experimental sites, and the range in tree crown dimensions measured are shown in Table 1.

Ground Measurement of Olive Crown Dimensions

The cV of each olive tree was calculated from the coordinates of the tree silhouette. The tree-cV was divided into eight cV-sectors generated by eight equidistant trapezoids which were revolved around the central-vertical axis of the tree. The volumes corresponding to the 45° revolution of each trapezoid were calculated using the second Pappus-Guldinus theorem (Selby, 1973), and summed to obtain the tree-crown volume. The coordinates of each trapezoid silhouette were measured by placing a large ruler vertically at constant intervals from the center of the tree to the perimeter of the orthogonal tree-crown projection, and visually determining the interception of the foliage boundaries with the ruler, in each of four positions per trapezoid (Fig. 1a).

To measure the cA of individual olive trees, the perimeter of the orthogonal projection of the tree crown was marked onto the soil surface with a pole provided with a leveling bubble in eight points, drawing eight equidistant transects from the center of the tree (Fig. 1b). The projected olive crown area in the horizontal plane was calculated as the sum of the areas of circular sectors for each transect.

When the olive trees were formed with a single trunk and regular crowns (all trees in the olive orchard Alameda del Obispo and younger trees in El Tobazo), the crown of the olive trees was divided into four tree-crown sectors for determinations of olive crown volume and projected crown area.

Ground Measurement of Crown Transmittance and Leaf Area Index of Individual Olive Trees

Crown transmittance of individual olive trees was measured using the LAI-2000 plant canopy analyzer (PCA) (Li-Cor,

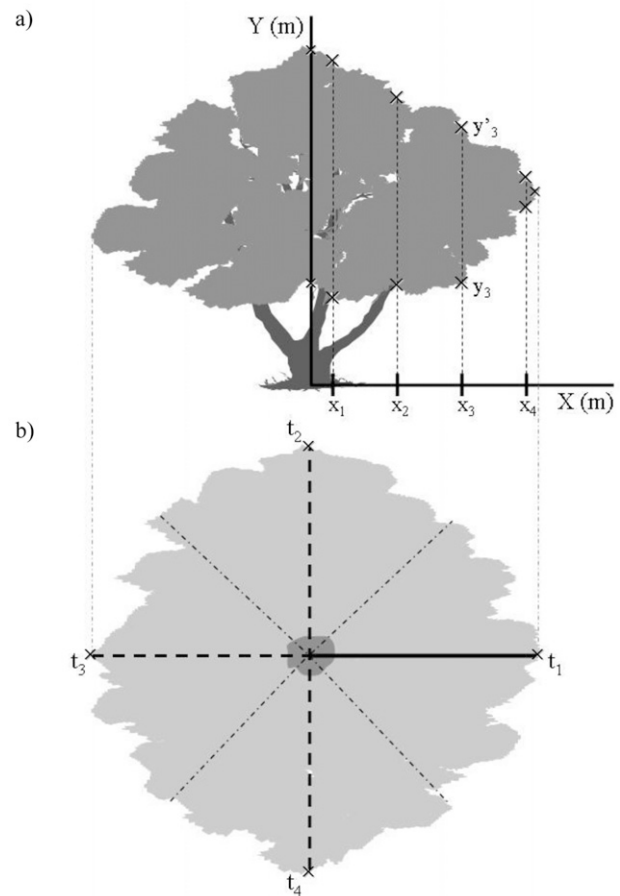


Fig. 1. (a) Description of the technique employed in measuring olive crown volume, crown transmittance, and leaf area index (LAI) of individual olive trees. X's are the points at ground level where the crown silhouette and the transmittance using plant canopy analyzer (PCA) were measured. The scheme refers to one of the four orthogonal sectors into which each one-trunk tree was divided (figure adapted from Iniesta et al., 2009). (b) Determination of the projected crown area in olive trees. The scheme shows the four transects (T's) and corresponding areas into which each one-trunk tree was divided. For details, see text (Materials and Methods).

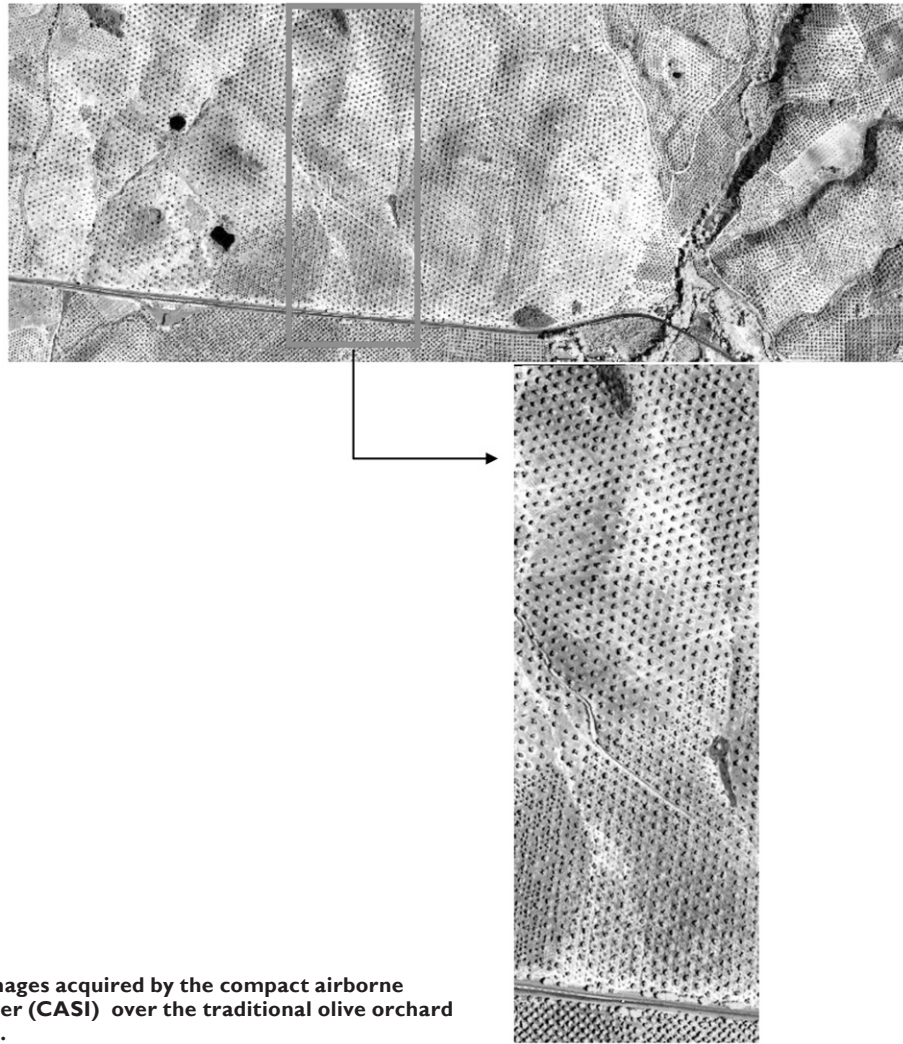


Fig. 2. Example of images acquired by the compact airborne spectrographic imager (CASI) over the traditional olive orchard ('El Tobazo') in 2003.

Lincoln, NE) in July 2003 and 2004. This device measures the fraction of diffuse incident radiation transmitted through a plant canopy (or *gap fraction*), by taking the ratio of the below-to the corresponding above-canopy radiation measurements. For that purpose it has a set of optical sensors that simultaneously measure diffuse radiation in five ranges of zenith angles (for detailed description see Welles and Norman, 1991). For each zenith angle (θ), radiation transmittance [$T(\theta)$] through the plant canopy is determined by

$$T(\theta) = e^{-G(\theta) \times \text{LAD} \times S(\theta)} \quad [1]$$

where $G(\theta)$ is the G -function, a fraction of leaf area projected toward angle θ , LAD is the leaf area density ($\text{m}^2 \text{-leaf m}^{-3} \text{-canopy}$), and $S(\theta)$ is the path length through the plant canopy for each angle θ (m). The LAD is obtained rearranging Eq. [1] and by numerical integration over the range of zenith angles measured by the PCA (Miller, 1967).

The leaf area density of individual olive trees (LAD_O) was determined using measurements of diffuse radiation transmittance in 32 (or 16 for one-trunk trees) points at the soil level, in the same positions used to determine trapezoid silhouettes (Fig. 1a). In each point, diffuse radiation transmittance was measured twice, just before sunrise and sunset to avoid direct

radiation. In all these measurements, only the reading of the PCA sensor measuring in vertical zenith angle ($0^\circ\text{--}12^\circ$) was used. Under these conditions, the LAD in each measurement point (p) can be solved numerically as

$$\text{LAD}_p = \frac{-\ln\left[\left(\frac{B}{A}\right)_p\right]}{G S_p} \quad [2]$$

where LAD_p is the leaf area density ($\text{m}^2 \text{m}^{-3}$) calculated from a single point p , $(B/A)_p$ is the measured vertical beam transmittance in the point p (T_p , dimensionless), being B and A diffuse radiation measurements below and above the crown canopy at that point, G is the G -function for zero zenith angle (dimensionless) that for an olive tree is 0.77 (Mariscal et al., 2000), and S_p is the canopy depth (the path length of the vertical beam in the crown canopy) at the point p (m), measured when determined the coordinates of the trapezoid silhouettes (Fig. 1a).

The LAD_O was obtained as the weighted average of the LAD measurements in the 32 (or 16) points per tree. First, the leaf area density of each trapezoid (LAD_p) was calculated as the average of the LAD measurements in the four points per transect weighted by the respective canopy depths, S_p . Afterward, LAD_O was obtained as the weighted average of the LAD_p values, considering the respective circular sector areas for each transect.

The leaf area index per individual olive trees (LAI_O , $\text{m}^2 \text{m}^{-2}$) was calculated using:

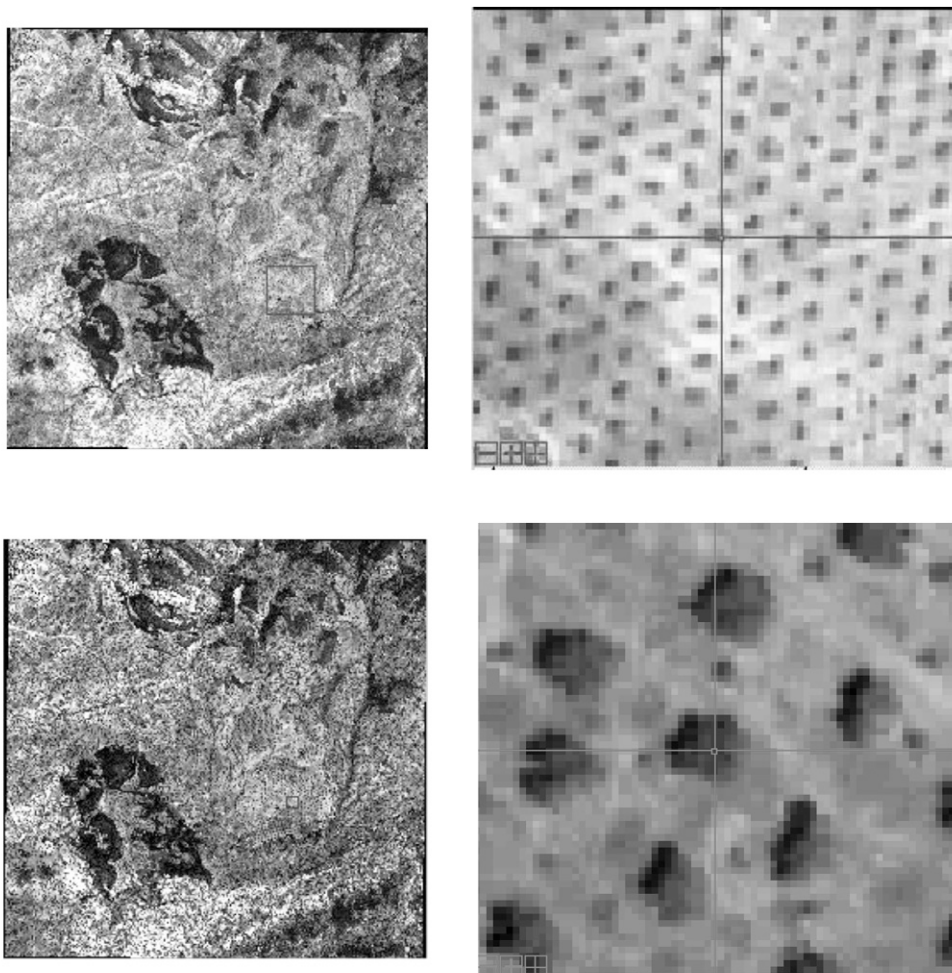


Fig. 3. Example of hyperspectral (above) and panchromatic (below) images acquired by the QuickBird satellite sensor over the traditional olive orchard ('El Tobazo') in 2003.

$$LAI_0 = \frac{LAD_0 \times cV}{cA} \quad [3]$$

where cV and cA are the crown volume and orthogonally projected crown area, respectively, of individual olive trees, both measured as indicated in the previous section. Therefore, LAI can be defined for individual trees as the crown leaf area per unit of projected crown area.

Because the optical sensor sees not only the leaves but also branches and stems, the equivalent terms for individual trees using the PCA will be plant area density (PAD) and plant area index (PAI). In olive trees grown in the field, >90% of the plant surfaces correspond to leaves (Villalobos et al., 1995), so PAD and PAI can be approximated to LAD and LAI. The crown transmittance of individual olive trees (T_O , dimensionless) was obtained as the average of the transmittance measurements (T_p) on each olive tree.

Remote Sensing Imagery

Two high-spatial resolution sensors were used in this study. The CASI hyperspectral sensor was flown over the two experimental sites at a flight altitude of 2250 m in July 2003. It provided images at 1-m spatial resolution in seven spectral bands centered at 490.7, 550.6, 670.3, 700.7, 750.1, 775, and 800 nm, with a bandwidth oscillating between 4 and 12 nm. The

uncalibrated images of CASI were converted into radiance using the calibration coefficients obtained in laboratory at the Centre for Research in Earth and Space Technology (CRESTech, Montreal, QB) and York University (Toronto, ON, Canada). The aerosol optical depth (AOD) at wavelengths 340, 380, 440, 500, 670, 870, and 1020 nm were measured using MicroTops II sun photometer (Solar Light Co., Philadelphia, PA) during the flights, to determine the AOD at 550 nm required for the atmospheric correction with CAM5S (O'Neil et al., 1997). Figure 2 depicts an example of the images obtained with the CASI sensor.

QuickBird images of the experimental site corresponding to the traditional olive plantation were acquired for July 2003 and August 2004. Hyperspectral images have a spatial resolution of 2.5 m and four spectral bands (blue, 450–520 nm; green, 520–600 nm; red, 630–690 nm; and near-infrared, 760–900 nm), and a panchromatic mode with 0.6-m pixel size with one single broad band (450–900 nm). Radiometric calibration of the images was made using the calibration coefficients provided by DigitalGlobe (DigitalGlobe, Longmont, CO) to obtain spectral radiance. Once processed, the radiance images were converted into reflectance images using the radiative transfer model MODTRAN (Spectral Sciences, Burlington, MA). Figure 3 depicts an example of multispectral and panchromatic images acquired with QuickBird.

Table 2. Values of the calibration parameters used in the algorithms for olive crowns detection (TD_LWS) and delineation (TD_GF_REF).

Algorithm	Parameter	Values	
		Hyperspectral image	Panchromatic image
TD_LWS	IMGSF	1	1.5
	TDS	25	20
	R2THS	0.98	0.98
	MNSF	1	1.5
	MSF	6	6
	ITER	25	25
	ETOL	0	0
TD_GF_REF	Simple Angle Interval	10	10
	Std Dev for vertex Smoothing	1	1

The CASI imagery was used at full resolution and also downsampled to simulate satellite spatial resolution. Spectral resampling was conducted that transformed hyperspectral CASI images into panchromatic images centered at 675 nm with 309.3 nm bandwidth and thus simulating QuickBird.

Determination of Tree Crown Dimensions from Remote Sensing Images

Determination of the projected surface of the olive crowns was made using the three sets of available images (hyperspectral CASI, panchromatic QuickBird, and simulated panchromatic image from CASI). The automatic local maximum refinement and delineation algorithm or LMRDA (Pouliot et al., 2002) was used for identification and delineation of the olive crown on the images. This algorithm is implemented in two steps. First, the individual trees were identified using the TD_LWS algorithm, which starts its search on the brightest pixel. Afterward, the olive crowns were delineated using the TD_GF_REF algorithm. Both models were used with the parameters values shown in Table 2. Olive trees in the intensive plantation were close (3.5 m in the row) that overlapped the crowns; therefore, single tree delineation was possible only in the traditional plantation.

The image-estimated crown volumes (cV) for individual olive trees in the traditional plantation were obtained from the image-estimated crown projection areas (cA), using the regression relationship (cV vs. cA) determined experimentally from ground measurements of crown volume and projected crown area in each olive tree.

Determination of Spectral Indices for Olive Trees from Remote Sensing Images

For each of the individual trees identified in the images, several spectral vegetation indices (SVIs) were determined from the two sets of hyperspectral images. The NDVI (Rouse et al., 1974), is defined as

$$NDVI = (R_{NIR} - R_{RED}) / (R_{NIR} + R_{RED}) \quad [4]$$

where $R_{NIR} + R_{RED}$ are the values of the reflectance in the near-infrared (R_{800nm}) and red (R_{690nm}) bands, respectively. The RDVI as proposed by Rougean and Breon (1995) is defined by

$$RDVI = (R_{NIR} - R_{RED}) / \sqrt{R_{NIR} + R_{RED}} \quad [5]$$

The SR (Jordan, 1969; Rouse et al., 1974), is defined by

$$SR = (R_{NIR} / R_{RED}) \quad [6]$$

and the MSR (Chen, 1996) is defined by

$$MSR = \frac{(R_{NIR} / R_{RED}) - 1}{\sqrt{(R_{NIR} / R_{RED}) + 1}} \quad [7]$$

The data sets obtained for each of these four SVIs were compared with the ground measurements of biophysical properties of olive trees by regression analysis (Steel and Torrie, 1960), applied at individual-level tree data.

RESULTS AND DISCUSSION

Determination of Olive Crown Dimensions from Remote Sensing Imagery

Figure 4 depicts the relationships between ground measured and image estimated olive orthogonal crown projection areas for the different remote sensing images evaluated (hyperspectral CASI-airborne, panchromatic CASI-airborne, and panchromatic QuickBird-satellite images). The best relationship obtained was with the analysis of the CASI hyperspectral images (Fig. 4a; linear regression equation $cA = 2.50 + 0.981 cA'$), presenting the highest determination coefficient ($r^2 = 0.82$; $P < 0.0001$), and the lowest root mean square error (RMSE = 4.8 m²). This result suggests an appropriate performance of the detection algorithms used, but also the quality of the information provided by the images with high spatial resolution (1 m) and narrow-band information.

The analysis of the panchromatic QuickBird-simulated images from hyperspectral CASI images enabled the evaluation of the effects caused by the lower spectral resolution on the prediction of the tree crown projected area. The estimation of olive crown projected area by the analysis of CASI panchromatic images (Fig. 4b) showed a slightly worse performance ($r^2 = 0.76$, and RMSE = 5.6 m²) than using CASI hyperspectral images, explained by the loss of information when resampling from multispectral to simulated panchromatic images. The results obtained from analysis of QuickBird panchromatic images (Fig. 4c) resulted in the worst prediction of the values of the olive crown projected area ($r^2 = 0.65$, and RMSE = 6.2 m², for years 2003 and 2004), as expected, although statistically significant ($P < 0.0001$).

Figure 5 depicts the relationships between ground measured and image estimated olive crown volumes for the different remote sensing images evaluated. The best relationship obtained was with the analysis of the CASI hyperspectral images (Fig. 5a), yielding $r^2 = 0.87$ ($P < 0.0001$) with RMSE = 8.4 m³ (linear regression equation $cV = 3.00 + 1.024 cV'$). This result suggests an appropriate performance of the estimation of the olive crown projection area by CASI hyperspectral images, discussed in the previous step, as well as the adequacy of the relationship between crown volume and crown projected area of the olive trees in the traditional plantation, presented in Fig. 6a.

The relationships between cV and cA obtained from ground measurements of individual olive trees in the two experimental sites (olive orchards El Tobazo and Alameda del Obispo) are shown in Fig. 6a, and for different types of olive orchards evaluated (Table 1) in Fig. 6b. The regression equation for the

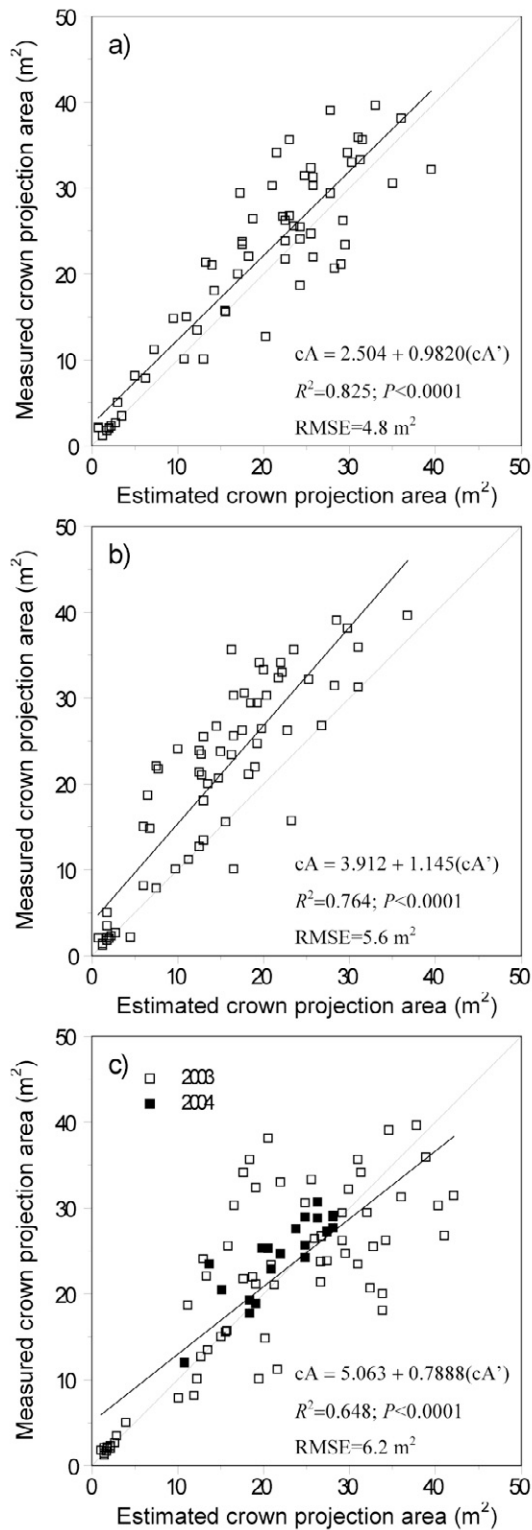


Fig. 4. Relationships between ground measured (vertical axis; crown area, cA) and image-estimated (horizontal axis; image-estimated crown projection area, cA') area of the orthogonal crown projection (m²) for individual olive trees using (a) hyperspectral compact airborne spectrographic imager (CASI) images, (b) panchromatic CASI airborne images, and (c) panchromatic QuickBird satellite images. Solid lines and accompanying statistics for (a), (b), and (c) describe linear regression relationships. Dashed lines indicate theoretical 1:1 relationships. Data from the traditional olive orchard ('El Tobazo').

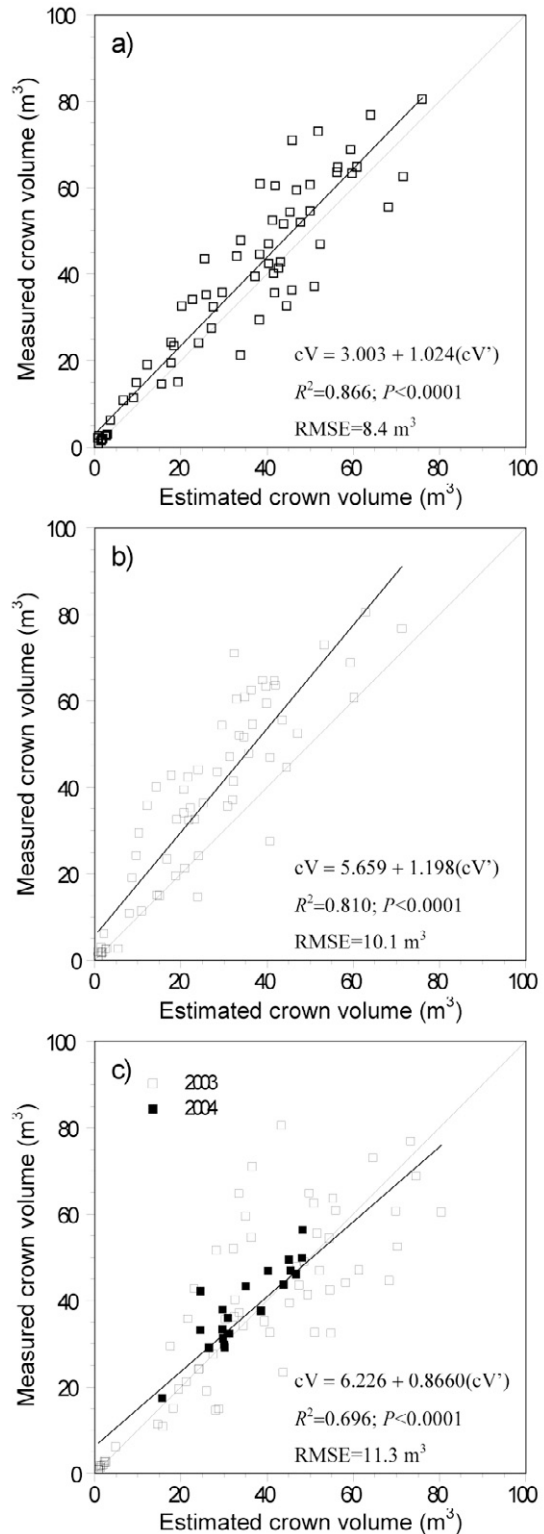


Fig. 5. Relationships between ground measured (vertical axis; crown volume, cV) and image-estimated (horizontal axis; image-estimated crown volume, cV') olive crown volume (m³) for individual trees using (a) hyperspectral compact airborne spectrographic imager (CASI images), (b) panchromatic CASI airborne images, and (c) panchromatic QuickBird satellite images. Solid lines and accompanying statistics for (a), (b), and (c) describe linear regression relationships. Dashed lines indicate theoretical 1:1 relationships. Data from the traditional olive orchard 'El Tobazo'.

Table 3. Determination coefficients (r^2) between the ground-measured crown transmittance ($-\ln T_O$) and plant area index of individual olive trees (PAI_O), and the corresponding values of the different spectral vegetation indices (SVIs) obtained from hyperspectral images using compact airborne spectrographic imager (CASI) airborne and QuickBird satellite sensors (NDVI, normalized difference vegetation index; RDVI, renormalized difference vegetation index; SR, simple ratio; MSR, modified simple ratio).

SVI	Crown transmittance ($-\ln T_O$)		Plant area index (PAI_O)	
	CASI image†	QuickBird image‡	CASI image	QuickBird image
NDVI	0.740	0.489	0.614	0.353
RDVI	0.750	0.500	0.618	0.371
SR	0.706	0.492	0.566	0.353
MSR	0.728	0.492	0.593	0.354

† Data from the olive orchards 'El Tobazo' and 'Alameda del Obispo' (year 2003).

‡ Data from the olive orchard 'El Tobazo' (years 2003 and 2004).

olive orchard El Tobazo shown in Fig. 6a was compared against ground measurements of cV and cA in a broad range of olive crown sizes, including different olive varieties, tree densities, and trunks per tree (Table 1), in Fig. 6b. That comparison suggests that this empirical relationship might be used for olive orchards with similar characteristics to that depicted in Fig. 6a, which are quite common in the region. It also suggests that large error in the determination of crown size can be introduced if tried to apply for specialized type of olive orchards, such as very-high density plantations with olive trees forming hedgerows, or for overlapped crowns, for example, intensive orchard Alameda del Obispo, Fig. 6a, or for large crowns with pruning adapted to table olive, for example, traditional orchard 'El Huerto', Fig. 6b. For these specific situations a new relationship cV vs. cA must be determined for a successful implementation of the methodology described in this manuscript.

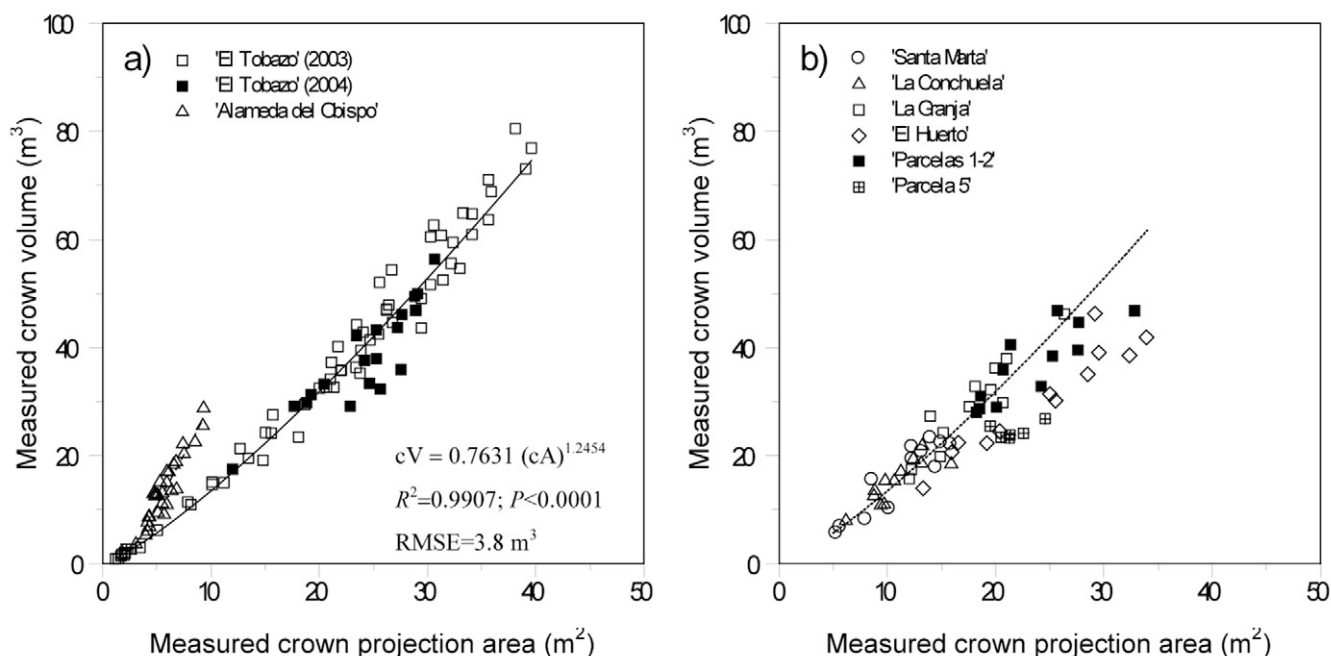


Fig. 6. Relationships between ground-measured olive tree crown volume (cV; m^3) and projected crown area (cA; m^2) for (a) experimental olive orchards 'El Tobazo' and 'Alameda del Obispo', and (b) different olive orchards typical of Andalusia (see Table 1). Solid line and summary statistics in (a) describe regression relationship obtained for the traditional plantation 'El Tobazo'. Dashed line in (b) represents the regression equation $cV = 0.763 \times cA^{1.245}$ obtained for the orchard 'El Tobazo'. (Olive orchard 'Alameda del Obispo': intrarow distance between trees of 0.35 m, with overlapping crowns).

Table 4. Summary of the ground-measured crown transmittance ($-\ln T_O$) and plant area index of individual olive trees (PAI_O) in the traditional ('El Tobazo', years 2003 and 2004) and intensive ('Alameda del Obispo', year 2003) olive orchards.

Olive orchard	Crown transmittance ($-\ln T_O$)		Plant area index (PAI_O)	
	range values	average (stdev)	range values	average (stdev)
Traditional	0.28–1.92	1.17 (0.34)	0.36–2.90	1.74 (0.53)
Intensive	0.98–2.85	2.16 (0.54)	1.08–3.70	2.66 (0.69)

The estimations of olive crown volume using panchromatic QuickBird-simulated images from hyperspectral CASI images (Fig. 5b) yielded lower r^2 ($=0.81$) and higher RMSE ($=10.1 m^3$) values, that is explained by the loss of information when resampling of CASI images to the QuickBird-simulated images for determination of the olive tree crown projection area. The results obtained from analysis of QuickBird panchromatic images (Fig. 5c) resulted in worse predictions of olive crown volumes ($r^2 = 0.70$, and RMSE = $11.3 m^3$, for years 2003 and 2004), although statistically accurate ($P < 0.0001$).

Determination of Olive Crown Transmittance

Determination coefficients (r^2) between ground measurements of olive crown transmittance and the different SVIs evaluated from two sets of hyperspectral images, CASI and QuickBird, are given in Table 3. It can be observed that the four indices (NDVI, RDVI, SR, and MSR) presented a better estimation of the crown transmittance with the CASI airborne sensor (r^2 ranging between 0.71 and 0.75, $P < 0.0001$, for SR and RDVI, respectively) compared to the QuickBird satellite sensor (r^2 ranging between 0.49 for NDVI and 0.50 for RDVI; $P < 0.0001$). Table 4 shows the summary of ground-measured values of the olive crown transmittance for traditional (El Tobazo) and intensive (Alameda del Obispo) olive orchards evaluated.

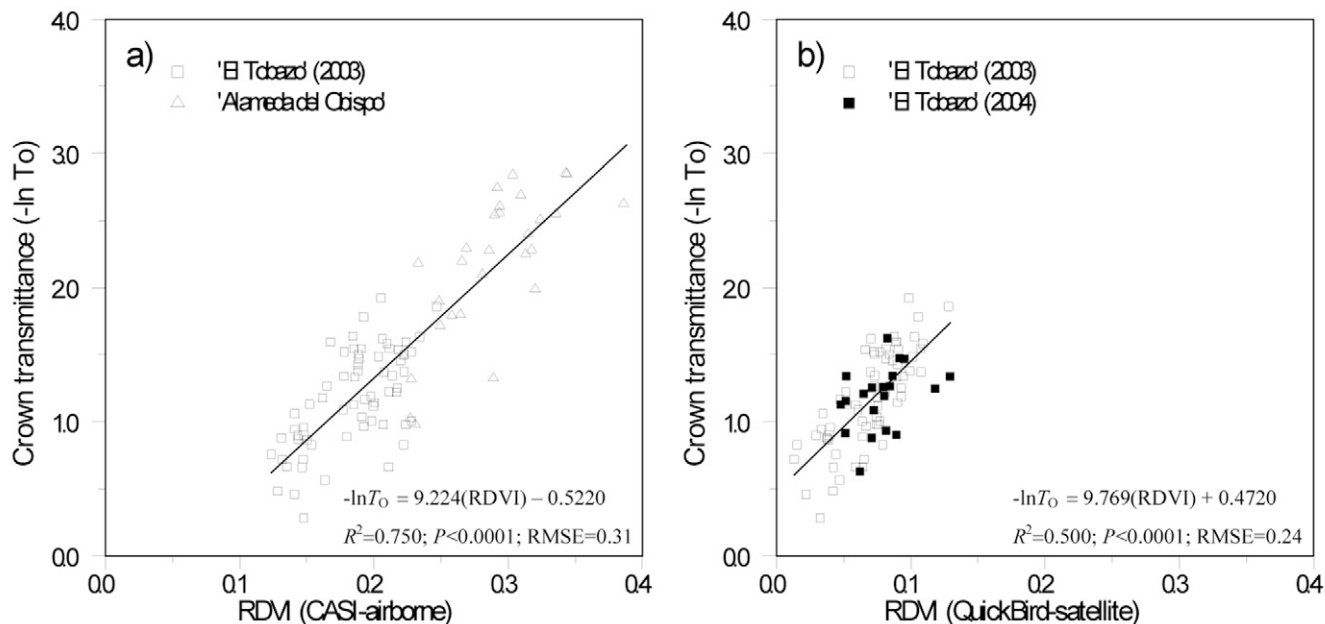


Fig. 7. Relationships between ground-measured crown transmittance ($-\ln T_o$; vertical axis) and renormalized difference vegetation index (RDVI) (horizontal axis) for individual olive trees using (a) compact airborne spectrographic imager (CASI) images and (b) QuickBird satellite hyperspectral images. Solid lines and summary statistics in both (a), and (b) describe linear regression relationships.

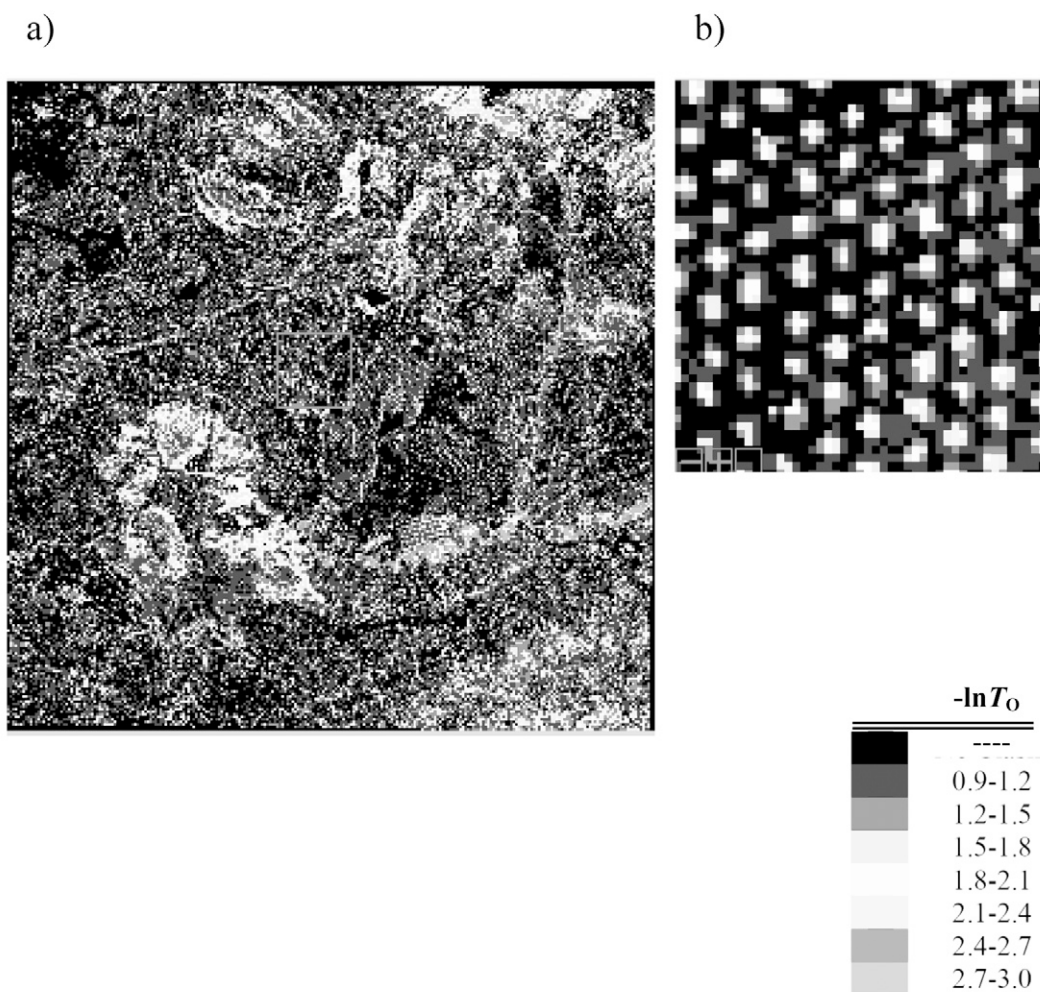


Fig. 8. (a) Mapping olive crown transmittance in a large (8 by 8 km) area from QuickBird satellite image in 2003 and (b) Detailed view of the differences in crown transmittance of individual olive trees over the traditional olive orchard (El Tobazo) in 2003 from QuickBird satellite image.

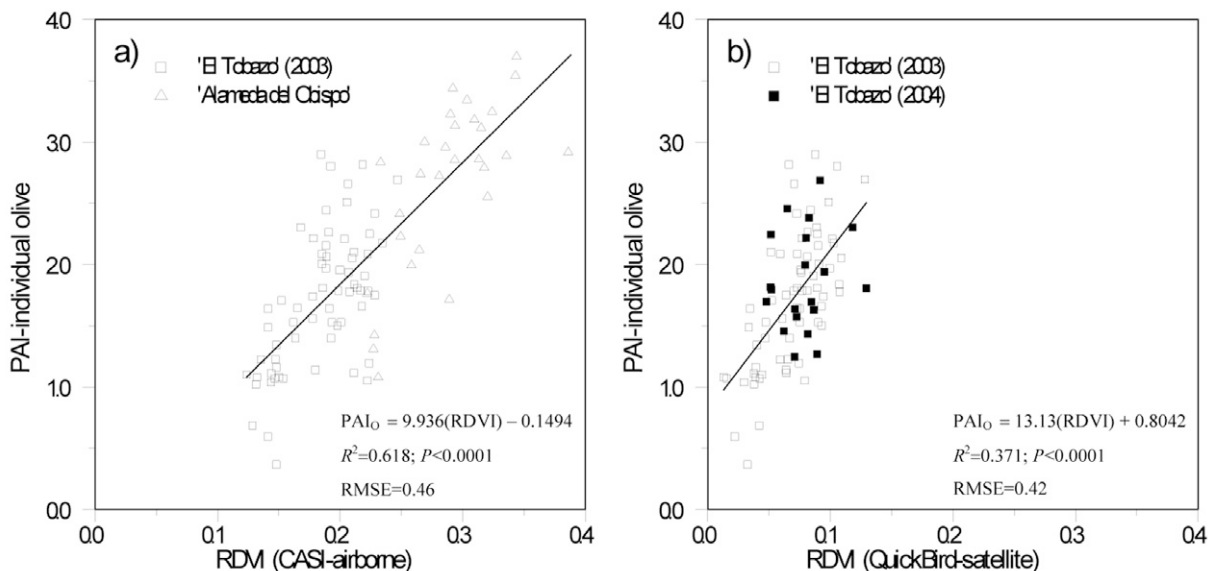


Fig. 9. Relationships between ground-measured plant area index (plant area index of individual olive trees, PAI_O) and renormalized difference vegetation index (RDVI) for individual olive trees using (a) compact airborne spectrographic imager (CASI) and (b) QuickBird satellite hyperspectral images. Solid lines and summary statistics in both (a) and (b) describe linear regression relationships.

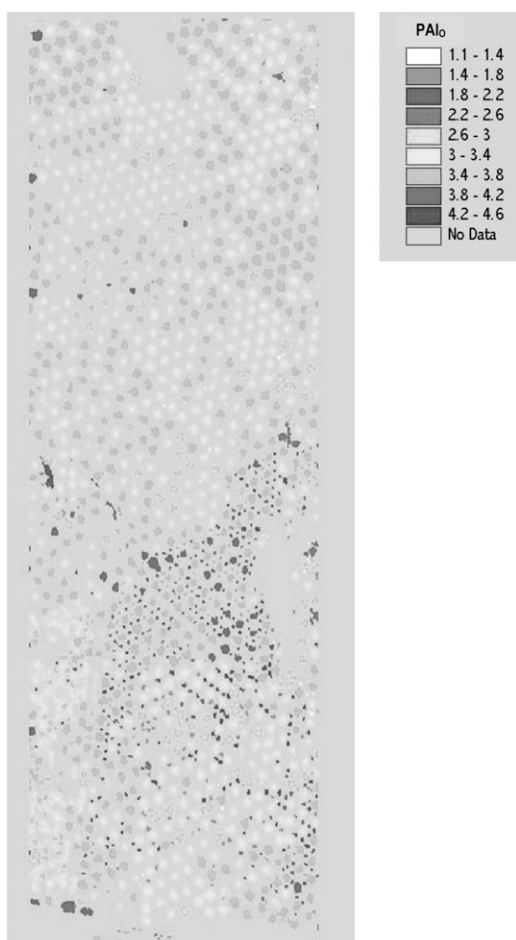


Fig. 10. Example of evaluation of olive trees canopy at farm scale by remote sensing. Detailed view of the differences in plant area index (PAI) of individual olive trees over the traditional olive orchard ('El Tobazo') in 2003. Plant area index of individual olive trees (PAI_O) values were obtained from renormalized difference vegetation index (RDVI) values from compact airborne spectrographic imager (CASI) images, using the regression equation between ground-measured PAI_O and RDVI from CASI-airborne images for individual olive trees (see Fig. 9a).

Figure 7 shows the relationships between these measured values of olive crown transmittance and one of those indices, RDVI, for both sensors. The best relationship obtained was with RDVI for CASI-airborne sensor ($-\ln T_o = -0.522 + 9.22 \text{ RDVI}$; $r^2 = 0.75$; $\text{RMSE} = 0.31$; Fig. 7a) compared with QuickBird-satellite sensor ($-\ln T_o = 0.472 + 9.77 \text{ RDVI}$; $r^2 = 0.50$; $\text{RMSE} = 0.24$; Fig. 7b).

Results in Table 4 and Fig. 7 show the ability of capturing the variability in the olive crown transmittance using SVIs derived from CASI or QuickBird images. This is illustrated in Fig. 8a, where the variability in crown transmittance in a large (8 by 8 km²) area, using the regression equation between ground-measured crown transmittance and RDVI from QuickBird images for individual olive trees, is shown. A zoom of such image allows identification of differences in the crown transmittance of the olive trees (Fig. 8b). These results demonstrate the application of this methodology for mapping olive crown transmittance in large areas, and at orchard scale where we can see the differences among individual olive trees.

Determination of Plant Area Index of Individual Olive Trees from Remote Sensing Imagery

Table 3 summarizes the correlation between the ground measurements of plant area index of individual olive trees (PAI_O) and the different SVIs evaluated from CASI (r^2 ranging from 0.57 to 0.62, $P < 0.0001$, for SR and RDVI, respectively), and QuickBird (r^2 ranging between 0.35 for NDVI and 0.37 for RDVI; $P < 0.0001$) hyperspectral images. It is apparent that remote sensing enables a moderate determination of PAI_O better with CASI images. The best relationship obtained was with RDVI for CASI-airborne sensor ($PAI_O = -0.149 + 9.94 \text{ RDVI}$; $r^2 = 0.62$; $\text{RMSE} = 0.46$; Fig. 9a) compared with QuickBird-satellite sensor ($PAI_O = 0.804 + 13.13 \text{ RDVI}$; $r^2 = 0.37$; $\text{RMSE} = 0.42$; Fig. 9b). The best estimations of PAI_O from CASI compared to QuickBird images were due to better spatial and spectral resolution of the airborne sensor as compared with the satellite imagery. Table 4 summarizes the ground-measured

values of the PAI in individual olive trees in the two different orchards evaluated (El Tobazo and Alameda del Obispo).

Leaf area index, of which PAI is a good proxy since in adult olive trees more than 90% of plant surface correspond to leaves, is a key parameter in modeling agronomical and hydrological processes in olive orchards like, for instance, rainfall interception (Gómez et al., 2001), and radiation interception (Mariscal et al., 2000). These methods enable for determining and mapping of PAI of individual olive trees over large areas, using hyperspectral remote sensing images. Figure 10 shows an example of evaluation of PAI_O at orchard scale (El Tobazo) with the methodology proposed in this study, showing significant differences in the PAI_O between different areas of the olive orchard. Thus, these detailed PAI_O maps would provide useful information for agronomic and hydrological models and for an appropriate site-specific orchard management.

CONCLUSIONS

Overall, the spectral vegetation indices evaluated (NDVI, RDVI, SR, and MSR) combined with the tree crown projection area obtained from remote sensing imagery (CASI airborne and QuickBird satellite-based) enabled the characterization at individual tree scale of key biophysical indicators, such as crown size, crown transmittance, and LAI, of olive trees over large areas. Leaf area index and percent crown cover of canopy trees are key variables in many hydrological and ecophysiological models, governing several processes such as photosynthesis, transpiration, or rainfall interception. The methodology developed in this study enables for determining and mapping of LAI, crown transmittance, crown cover, and crown volume of individual olive trees at orchard scale and in large areas, and the validity of the methods used when applied to satellite images. Future studies should try to increase the accuracy in determination of biophysical indicators for individual olive trees.

ACKNOWLEDGMENTS

This work was funded by Spain's Ministerio de Educación y Ciencia, Projects AGL2002-04407-C03-02, AGL2009-13105-C01, and FEDER funds. We thank the owner and staff of the farm 'El Tobazo' for their support during the field measurements made in their property during this project.

REFERENCES

Barr, A.G., T.A. Black, E.H. Hogg, N. Kljun, K. Morgenstern, and Z. Nestic. 2004. Inter-annual variability in the leaf area index of a boreal aspen-hazelnut forest in relation to net ecosystem production. *Agric. For. Meteorol.* 126:237–255. doi:10.1016/j.agrformet.2004.06.011

Bréda, N.J.J. 2003. Ground-based measurements of leaf area index: A review of methods, instruments and current controversies. *J. Exp. Bot.* 54:2403–2417. doi:10.1093/jxb/erg263

Chen, J. 1996. Evaluation of vegetation indices and modified simple ratio for boreal applications. *Can. J. Rem. Sens.* 22:229–242.

Consejería de Agricultura y Pesca. 2010. Agricultural statistics. Available at <http://www.juntadeandalucia.es/agriculturaypesca/portal/servicios/estadisticas/index.html> (accessed September 2010; verified 11 Sept. 2011). Consejería de Agricultura y Pesca, Seville, Spain.

Cutini, A., G. Matteucci, and G.S. Mugnozza. 1998. Estimating of leaf area index with the Li-Cor LAI 2000 in deciduous forests. *For. Ecol. Manage.* 105:55–65. doi:10.1016/S0378-1127(97)00269-7

FAOSTAT. 2010. Agricultural statistics. Available at <http://faostat.fao.org/site/567/DesktopDefault.aspx?PageID=567#ancor> (accessed September 2010; verified 11 Feb. 2011). FAO, Rome.

Fassnacht, K.S., S.T. Gower, M.D. MacKenzie, E.V. Nordheim, and T.M. Lillesand. 1997. Estimating the leaf area index of North Central Wisconsin forests using the landsat thematic mapper. *Remote Sens. Environ.* 61:229–245. doi:10.1016/S0034-4257(97)00005-9

Gómez, J.A., M. Battany, C.S. Renschler, and E. Fereres. 2003. Evaluating the impact of soil management on soil loss in olive orchards. *Soil Use Manage.* 19:127–134. doi:10.1079/SUM2002179

Gómez, J.A., J.V. Giraldez, and E. Fereres. 2001. Rainfall interception by olive trees in relation to leaf area. *Agric. Water Manage.* 49:65–76. doi:10.1016/S0378-3774(00)00116-5

Gower, S.T., and J.M. Norman. 1991. Rapid estimation of leaf area index in conifer and broad leaf plantations. *Ecology* 72:1896–1900. doi:10.2307/1940988

Haboudane, D., J.R. Miller, E. Pattey, P.J. Zarco-Tejada, and I. Strachan. 2004. Hyperspectral vegetation indices and novel algorithms for predicting green LAI of crop canopies: Modelling and validation in the context of precision agriculture. *Remote Sens. Environ.* 90:337–352. doi:10.1016/j.rse.2003.12.013

Iniesta, F., L. Testi, F. Orgaz, and F.J. Villalobos. 2009. The effects of regulated and continuous deficit irrigation on the water use, growth and yield of olive trees. *Eur. J. Agron.* 30:258–265. doi:10.1016/j.eja.2008.12.004

Johnson, L.F., D.E. Rozen, S.K. Youkhana, R.R. Nemani, and D.F. Bosch. 2003. Mapping vineyard leaf area with multispectral satellite imagery. *Comput. Electron. Agric.* 38:33–44. doi:10.1016/S0168-1699(02)00106-0

Jonckheere, I., S. Fleck, K. Nackaerts, B. Muys, P. Coppin, M. Weiss, and F. Baret. 2004. Methods for leaf area index determination. Part I: Theories, techniques and instruments. *Agric. For. Meteorol.* 121:19–35. doi:10.1016/j.agrformet.2003.08.027

Jordan, C.F. 1969. Derivation of leaf-area index from quality of light on the forest floor. *Ecology* 50:663–666. doi:10.2307/1936256

Laliberte, A.S., A. Rango, K.M. Havstad, J.F. Paris, R.F. Beck, and R. McNeely. 2004. Object-oriented image analysis for mapping shrub encroachment from 1937 to 2003 in southern New Mexico. *Remote Sens. Environ.* 93:198–210. doi:10.1016/j.rse.2004.07.011

Mariscal, M.J., F. Orgaz, and F.J. Villalobos. 2000. Modelling and measurement of radiation interception by olive canopies. *Agric. For. Meteorol.* 100:183–197. doi:10.1016/S0168-1923(99)00137-9

Miller, J.B. 1967. A formula for average foliage density. *Aust. J. Bot.* 15:141–144. doi:10.1071/BT9670141

Monsi, M., and T. Sacki. 1953. Über den Lichtfaktor in Pflanzengesellschaften und seine Bedeutung für die Stoffproduktion. *Jpn. J. Bot.* 14:22–52.

Norman, J.M., and G.S. Campbell. 1989. Canopy structure. p. 301–325. *In* R.W. Pearcy et al. (ed.) *Plant physiological ecology: Field methods and instrumentation*. Chapman and Hall, London.

O'Neil, N.T., F. Zagolski, M. Bergeron, A. Royer, J.R. Miller, and J. Freemantle. 1997. Atmospheric correction validation of CASI images acquired over the BOREAS Southern Study Area. *Can. J. Rem. Sens.* 23:143–162.

Pastor, M., M. García-Vila, M.A. Soriano, V. Vega, and E. Fereres. 2007. Productivity of olive orchards in response to tree density. *J. Hortic. Sci. Biotechnol.* 82:555–562.

Pouliot, D.A., D.J. King, D.G. Pitt, and F.W. Bell. 2002. Automated tree crown detection and delineation in high-resolution digital camera imagery of coniferous forest regeneration. *Remote Sens. Environ.* 82:322–334. doi:10.1016/S0034-4257(02)00050-0

Rougean, J.L., and F.M. Breon. 1995. Estimating PAR absorbed by vegetation from bidirectional reflectance measurements. *Remote Sens. Environ.* 51:375–384.

Rouse, J.W., R.H. Haas, J.A. Schell, D.W. Deering, and J.C. Harlan. 1974. Monitoring the vernal advancements and retrogradation of natural vegetation. NASA/GSFC, Greenbelt, MD.

Selby, S.M. 1973. CRC Standard mathematical tables. CRC Press, Cleveland, OH.

Steel, R.G.D., and J.H. Torrie. 1960. Principles and procedures of statistics. McGraw-Hill, New York.

Stenberg, P., S. Linder, H. Smolander, and J. Flower-Ellis. 1994. Performances of the LAI-2000 plant canopy analyser in estimating leaf area index of some Scots pine stands. *Tree Physiol.* 14:981–995.

Turner, D., W. Cohen, R. Kennedy, K. Fassnacht, and J. Briggs. 1999. Relationships between leaf area index and Landsat TM spectral vegetation indices across three temperate zone sites. *Remote Sens. Environ.* 70:52–68. doi:10.1016/S0034-4257(99)00057-7

Villalobos, F.J., F. Orgaz, and L. Mateos. 1995. Non-destructive measurement of leaf area in olive (*Olea europaea* L.) trees using a gap inversion method. *Agric. For. Meteorol.* 73:29–42. doi:10.1016/0168-1923(94)02175-J

Watson, D.J. 1947. Comparative physiological studies in the growth of field crops. I. Variation in net assimilation rate and leaf area between species and varieties, and within and between years. *Ann. Bot. (London)* 11:41–76.

Weiss, M., F. Baret, G.J. Smith, I. Jonckheere, and P. Coppin. 2004. Review of methods for in situ leaf area index (LAI) determination: Part II. Estimation of LAI, errors and sampling. *Agric. For. Meteorol.* 121:37–53. doi:10.1016/j.agrformet.2003.08.001

Welles, J.M., and J.M. Norman. 1991. Instrument for indirect measurement of canopy architecture. *Agron. J.* 83:818–825. doi:10.2134/agronj1991.00021962008300050009x